ROYAL SOCIETY
OF CHEMISTRY

PAPER

Check for updates

Immobilization of molecular complexes on graphitized carbon cloth as stable and hybrid electrocatalysts for enhanced hydrogen evolution reaction and oxygen evolution reaction†

Ram Murthy [iD] and Sundaresan Chittor Neelakantan [iD] *

The search for an environment friendly, sustainable and cost-effective catalyst used in electrochemical water splitting *via* the hydrogen evolution reaction (HER) has generated considerable interest in renewable energy research worldwide. In the current study, we report cost-effective and easily synthesizable 2-thioureidobenzothiazole (BTT) metal complexes (M = Pd, Co, Ni) as dual and efficient electrocatalysts for HER and OER applications in acidic and alkaline conditions, respectively. The hybrid molecular catalysts were synthesized by integrating transition metal complexes with graphitized carbon cloth (GrCC) as the carbon support. The pristine Pd(II)BTT complex exhibited enhanced hydrogen evolution activity with an applied overpotential value of 178 mV (*vs.* RHE) and a significantly lower Tafel slope value of 73.74 mV per decade in 0.5 M H_2SO_4 solution. The high catalytic activity of the Pd(II)BTT complex can be ascribed to the strong affinity of the Pd metal ion towards H_2. The Ni(II)BTT/GrCC hybrid catalyst for the HER exhibited an overpotential of 335 mV (*vs.* RHE) to drive a current density of 10 mA cm^{-2} and was found to be superior *vis-a-vis* the pristine nickel complex. The enhanced catalytic activity of the hybrid catalyst is due to the conducting and porous nature of the graphitized carbon cloth. For OER activity, the pristine Ni(II)BTT complex exhibited a very low overpotential value of 250 mV to drive a current density of 10 mA cm^{-2} and gave a low Tafel slope value of 93 mV per decade. The cost-effective and robust nickel complex as a novel electrocatalyst was found to be very effective for both HER and OER applications. This work paves the way for a new avenue to combine molecular catalysts with effective carbon supports for energy storage applications.

1 Introduction

Currently worldwide, there is an unprecedented awareness and there are efforts to reduce the carbon footprint by substituting fossil fuels with a very sustainable and economically viable green renewable energy source. Though wind and solar energy systems are evolving to provide viable and efficient alternative clean energy resources, they are beset with certain limitations. In this context, hydrogen has tremendous potential as a promising future energy currency and is prognosticated as a very prominent next-generation renewable energy source.[1] The hydrogen evolution reaction (HER) and oxygen evolution reaction (OER) have been recognised as clean and sustainable ways of generating green energy.[2] Researchers have devoted

significant and sustained effort to develop inexpensive, durable, and efficient electrocatalysts for water splitting reactions.

Ideal electrocatalysts would involve small overpotential and possess fast reaction kinetics to produce hydrogen. To date, platinum (Pt)-based electrocatalysts are considered as the gold standard for the HER, owing to their strength of Pt–H bond and faster facile kinetics.[3] Exorbitant cost and insufficient reserves of platinum have hindered industrial scalability. Palladium is emerging as a very promising alternative to platinum owing to its availability, relatively lower cost and good catalytic activity.[4] Currently, palladium metal is extensively utilized in the automotive industry to lower the toxicity of emissions from the combustion engine.[4] Many non-precious metals such as Co,[5,6] Ni,[7] and Fe are preferred for water electrolysis due to their affordable cost and abundance on the earth's crust.[8,9] Various factors determine the efficiency of the electrocatalyst, *i.e.*, electrode modification, nature of the electroactive material, presence of a carbon support, the porosity of the material, *etc.* Transition metals are preferred because of their ease of

Department of Chemistry, Sri Sathya Sai Institute of Higher Learning,
Brindavan Campus, Kadugodi, Bengaluru – 560067, India.
E-mail: cnsundaresan@sssihl.edu.in

† Electronic supplementary information (ESI) available. See DOI: **https://doi.org/10.1039/d2ma00764a**

synthesis, broad applicability, and functionality in neutral, alkaline and acidic conditions.

2-Thioureidobenzheteroazoles (BTZs) undergo chelation with metal atoms through thiazole sulphur and thioureido sulphur atoms to give a stable metal complex. The synthesized metal complexes with the general formula $[M(C_8H_8N_6S_6)_2Cl_2]^{+2}$ (M = Pd, Co, and Ni) have been used to evaluate HER & OER activity. The Pd complex has square planar geometry, while both Co and Ni metal complexes have tetrahedral geometry.[10] In order to further enhance the activity of the molecular catalyst, the metal complexes were incorporated into a carbon support.

Various carbon supports, such as carbon nanotubes[11] (MWCNTs, SWCNTs), fullerene,[12] graphene,[13] carbon fiber cloth,[14] and porous carbon,[15] are favored for electrocatalytic applications due to their excellent electrochemical stability, conductivity[16] and favorable mass-transport properties. These carbon supports have shown remarkable electrochemical efficiency in numerous batteries and supercapacitors.[17] The conventional strategy involves the modification of the electrode by drop casting the catalyst on the surface of the electrode. This strategy suffers from the problem of leaching due to the fragile linkage between the molecular catalyst and electrode surface. To overcome these limitations, molecular catalysts were integrated into carbon supports to enhance the HER activity (Fig. 2).

In this study, graphitized carbon cloth (CC) has been used as a carbon support owing to graphene's excellent electronic conducting nature and the porous nature of the carbon cloth for HER activity. The current study reports a method to synthesize low-cost transition metal complexes as dual electrocatalysts for HER and OER applications. We demonstrate a simple method of integrating transition metal complexes with graphitized carbon cloth as a carbon support for enhanced hydrogen and oxygen evolution in acidic and alkaline conditions, respectively. With this motive, Co, Ni, and Pd metal complexes of 2-thioureidobenzothiazoles were chosen as electroactive materials for studying hydrogen evolution reactions and oxygen evolution reactions.

2 Results and discussion

Pd, Co, and Ni coordination complexes were prepared under alkaline conditions (Fig. 1). The procedure detailing the synthesis and characterization have been described in S2 and S3 (ESI†). The metal complexes were immobilized on carbon cloth by a simple drop-casting method and dried at room temperature (Fig. 2). To confirm the successful immobilization of the complexes on the graphitized carbon cloth, X-ray photoelectron spectroscopy (XPS) measurements were performed (shown in Fig. 3). The XPS spectrum of the electrocatalyst immobilized graphitized carbon cloth exhibits two characteristic peaks of 335.5 eV and 337.8 eV corresponding to Pd 3d5/2 and Pd 3d3/2 metal (Table 1). The peak at 284.5 eV can be attributed to the sp2 hybridized carbon atoms.[18] In Fig. 3 and 4, the peak at 335.5 ± 0.2 eV can be attributed to Pd^{2+}, which can be quickly bonded to an oxygen atom.[18]
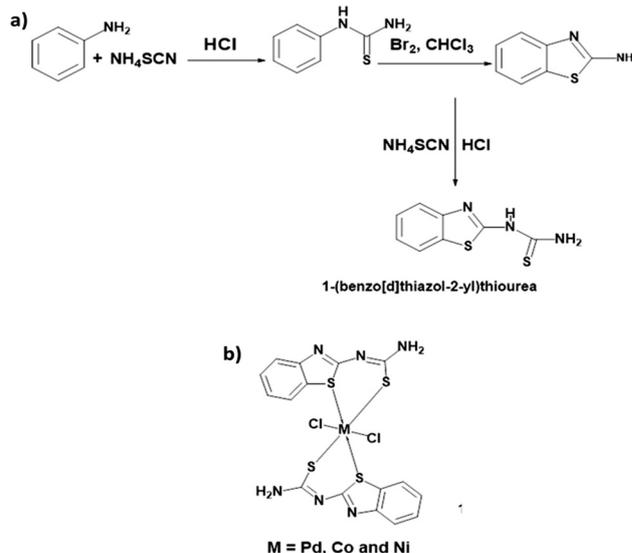

Fig. 1 (a) Synthetic route of the ligand 2-thioureidobenzothiazole and (b) general structure of the 2-thioureidobenzothiazole metal complex.

Comparing the XPS pattern of carbon cloth before and after the HER reaction, Fig. 3(a and b) show the used Pd(II)BTT complex, which is observed to show a decreased intensity at 343.88 eV (Table 1). In Fig. 4b, the Ni complex shows a characteristic peak at 853.7 eV, which can be attributed to Ni 2p3/2 (Ni^{2+}) present on the carbon cloth surface, and other peaks remain constant (Fig. S1, ESI†) (Table 1).

The FT-IR spectra of the metal complexes Pd(II)BTT, Co(II)BTT, and Ni(II)BTT are shown in Section S3 (ESI†). The bands at 1585 cm^{-1} and 755 cm^{-1} are due to thioamide stretching and bending vibrations, respectively. The band at 1629 cm^{-1} corresponds to the ν(N–H) bending of the ligand. The bands at 1132 cm^{-1}, 1184 cm^{-1}, and 996 cm^{-1} can be attributed to ν(C=S) for Pd(II), Co(II) and Ni(II) complexes, respectively.[10] The bands in the range of 740–755 cm^{-1} are attributed to ν(C–S–C) of the thiazole ring in all three complexes.[10] Complexation of the ligand with metals leads to a shift in the band to lower frequency, implying that the thiocarbonyl group is involved in complexing with the metal ion.

The UV-Vis absorbance spectra of 2-BTT and its complexes are provided in Fig. S2 (ESI†). From Fig. S2 (ESI†), the ligand shows a strong peak at 306 nm, but in the case of all the three complexes, there is a hypsochromic shift in the wavelength of the complex, revealing the complex formation. The electron transition observed is π–π* for the complex. In the case of all the three complexes, a hypsochromic shift from 306 nm to 290 nm is observed, depicted in Fig. S2 of the ESI.†

The electronic spectrum of the Pd complex exhibited two broad absorption bands at 28 089 cm^{-1} and 34 482 cm^{-1} corresponding to charge transfer bands. The peaks observed in the UV region reflect π–π* transition. The energy absorption of 32 679 cm^{-1} (306 nm) is due to the thiazole moiety of the ligand. The energy absorption band moves to further higher energy of 34 482 cm^{-1} implying complexation. The crystal field splitting energy (CFSE) values increase from 390 kJ mol^{-1}
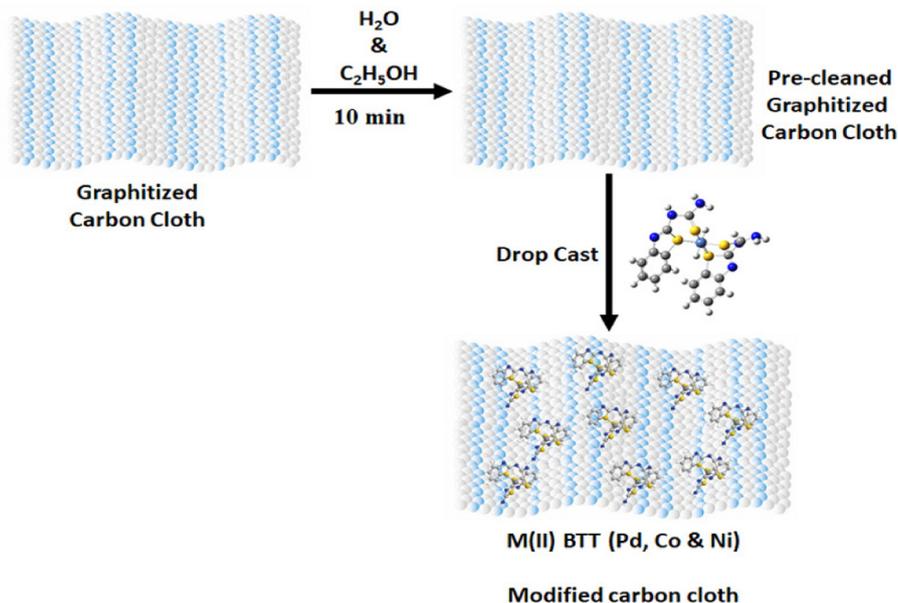
Fig. 2 Schematic representation of immobilization of M(II)BTT complexes onto graphitized carbon cloth (GrCC) at 298 K.
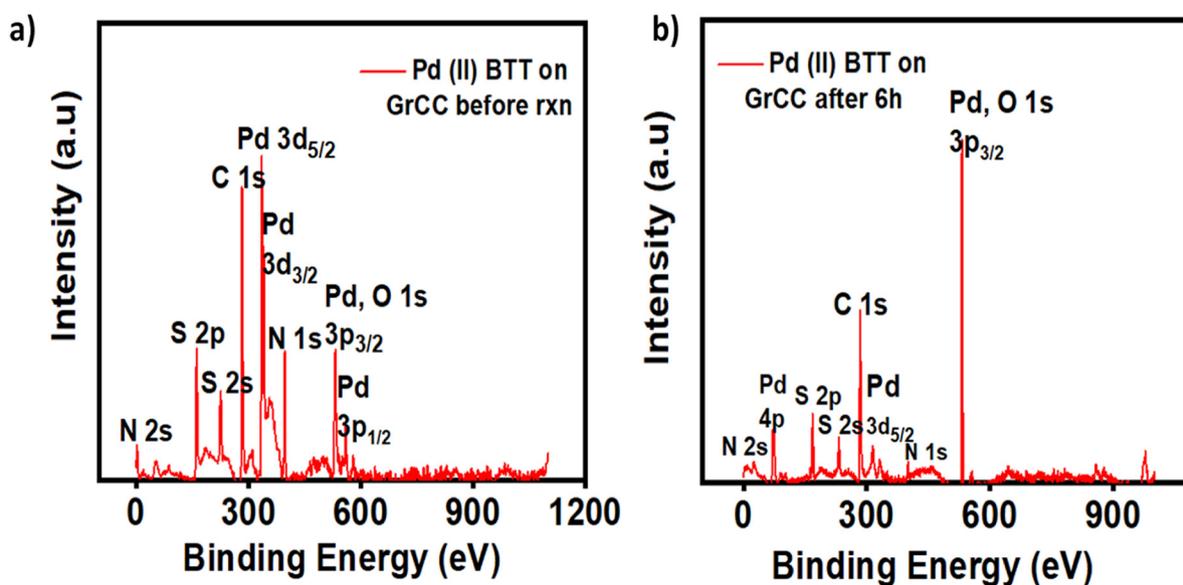

Fig. 3 XPS spectra of the Pd(II)BTT complexes. (a) Pd(II)BTT/GrCC hybrid electrocatalyst before the LSV test. (b) PdBTT/GrCC after the test (LSV 6 h stability).

(306 nm) to 412.47 kJ mol^{-1} (290 nm) reinforcing complex formation.[19]

Table 1 XPS peak positions obtained for the [Pd(BTT)/GrCC] catalyst before and after the reaction and Ni(II)BTT/GrCC catalyst before the reaction

Complex	Pd 3d5/2	Pd 3d3/2	Ni 2p	N 1s	S 4s	C 1s
[Pd(BTT)/GrCC] before rxn	335.2	337.5	—	400	164	284.5
[Pd(BTT)/GrCC] after 6 h	343.88	338.72	—	400.74	162.3	284.5
[Ni(BTT)/GrCC]	—	—	853.7	400	164	284.5

The thiocarbonyl moiety of the ligand undergoes strong chelation with the metal atom. The occupied sp$_x$ orbitals of the ligand interact with d$_{x^2-y^2}$ orbitals of the metal to form a σ bond. Furthermore, the metal donates an electron back to the ligand through π-back bonding. The back bonding is observed between the d$_{xz}$ orbital of the metal and p$_z$ of the ligand. This π-back bonding interaction results in increased mixing of the metal and ligand orbitals resulting in stable molecular complexes.[20]

2-Thioureidobenzothiazole metal complexes were subjected to morphological analysis by scanning electron microscopy as
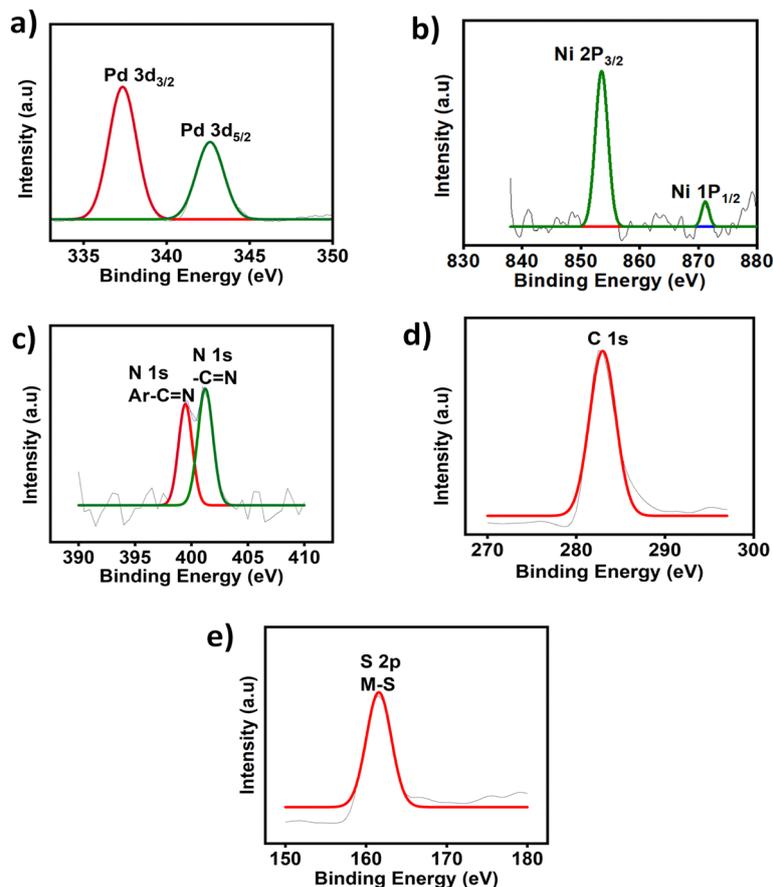
Fig. 4 XPS fine spectra. (a) Pd 3d 3/2, 5/2 of the Pd(II)BTT complex on carbon cloth (CC). (b) XPS peak Ni 2p 3/2 and Ni 1p 1/2 of the Ni(II)BTT complex on CC. (c) XPS peak of N 1s on GrCC. (d) XPS peak of C 1s on GrCC. (e) XPS peak of S 2p on GrCC.

shown in Fig. 5(a–d). The SEM images revealed the crystalline nature of the complexes. The palladium complex possesses a rod-like morphology while the nickel and cobalt complexes showed flaky morphology. The SEM images show increased space in the

Fig. 5 SEM images depicting the morphology of the M(II)BTT complexes. (a) Pd(II)BTT, (b) Co(II)BTT, (c) Ni(II)BTT, and (d) 2-thioureidobenzothiazole ligand.

complex compared to the 2-thioureidobenzothiazole ligand aiding in better adsorption and evolution of hydrogen in the process.

The thermal stability of the Pd, Co, and Ni(II) complexes of the 2-thioureidobenzothiazoles was investigated by thermogravimetric (TGA) analysis. Three prominent stages of decomposition were observed for each of the complexes (Fig. S5, ESI†). At temperatures ranging from 170 °C to 320 °C, the loss of HCl was observed.[10] Subsequently, the loss of the thioureido moiety was observed at a slightly higher temperature between 280 °C and 620 °C. A significant mass loss of the complex was observed at temperatures above 350 °C, and exo-effects with maxima at 370–390 °C were observed for the above decomposition. In the third stage of degradation, the ligand completely decomposes at the temperature range of 760–870 °C; endo effect is observed, and no further weight loss was observed with metal oxide (MO_x) as the final product[10] (Fig. S5, ESI†).

The magnetic properties of the 2-thioureidobenzothiazole metal complexes (Pd, Co, and Ni) were investigated using the vibrating sample magnetometer (VSM) technique. From Fig. S4 (ESI†), it was evident that the Pd(II)BTT and Ni(II)BTT complexes behave as diamagnetic due to the effective bonding of the unpaired electrons with the sulfur atoms of the ligand. In the case of the Co(II)BTT complex, ferromagnetic behavior is reflected in Fig. S4 (ESI†).
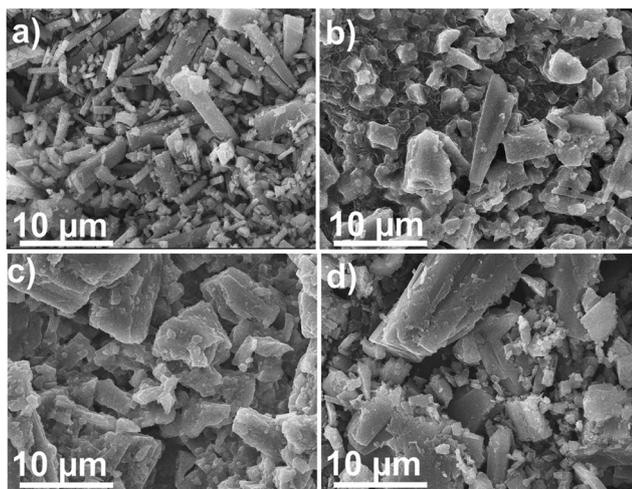
2.1 Electrochemical reaction

The 2-thioureidobenzothiazole metal complexes were evaluated for the hydrogen evolution reaction. The complexes were directly immobilized on graphitized carbon cloth (GrCC) by a simple drop-casting method and were dried at room temperature. The catalyst loading of 0.04 mg cm^{-2} and metal loading of 0.011 mg cm^{-2} were achieved on the carbon cloth. In the case of the pristine metal complexes, a catalyst loading of 0.282 mg cm^{-2} was attained on the electrode surface. The catalytic activity of the hybrid catalyst (M(II)BTT/GrCC, M = Pd, Co, and Ni) was compared to that of the pristine metal complexes (M(II)BTT) in 0.5 M H$_2$SO$_4$. The electrochemical measurements were obtained using a three-electrode system configuration with a glassy carbon electrode (GCE) as the working electrode, graphite rod as a counter electrode to avoid possible contamination by redeposition of Pt, and a saturated calomel electrode (SCE) as the reference electrode under continuous N$_2$ flow during the experiment. Graphitized carbon cloth (0.5 × 1 cm) of area 0.5 cm^2 was pretreated with deionized water and ethanol for 10 min sequentially. The pretreated GrCC was used to obtain a hybrid electrocatalyst for the HER.

2.1.1 Hydrogen evolution reaction. Linear sweep voltammetry measurements were obtained between 0 and −1 V at a scan rate of 50 mV s^{-1}, as shown in Fig. 6(a). The Pd(II)BTT complex exhibited an extremely low overpotential (η) of 178 mV (vs. RHE) compared to Pd(II)BTT/GrCC, which showed an overpotential (η) of 419 mV to drive a current density (j) of 10 mA cm^{-2} (Fig. 6a). The pristine Co(II)BTT and Ni(II)BTT complexes showed poor HER activity with overpotential values of 720 mV and 565 mV, respectively, to drive a current density of 10 mA cm^{-2}. In contrast, Co(II)BTT and Ni(II)BTT complexes on graphitized carbon cloth showed an improved activity with an η of 335 mV and 472 mV, respectively, to achieve a current

density of 10 mA cm^{-2}. The Pd/C material has an overpotential of 91 mV to achieve a current of current density of 10 mA cm^{-2}.[21] The activity of pristine Pd(II)BTT is better in comparison to Pd/C in 0.5 M H$_2$SO$_4$. LSV plots for the hybrid catalyst showed a strong indication of hydrogen evolution with high electrocatalytic current with increased bubble formation at the electrode/electrolyte interface. Electrocatalysis is intimately related to reducing Pd(II) to Pd(0) in the aqueous acidic solution. The decreased particle size of the Pd metal complex compared to the Co and Ni complexes significantly contributed to the enhanced HER activity.[22] The Pd complex in pristine form has better electrocatalytic activity due to the affinity of the palladium ion towards hydrogen and the effective ligand to metal charge transfer reaction.

The Pd(II)BTT/GrCC, Co(II)BTT/GrCC and Ni(II)BTT/GrCC showed a maximum current density of 44 mA cm^{-2}, 63 mA cm^{-2} and 110 mA cm^{-2} at 720 mV, respectively (Fig. 6a). In the case of the pristine complexes, Pd(II)BTT showed the maximum current density of 247 mA cm^{-2}, and the Co(II) and Ni(II) complexes of BTT showed a cumulative current density of 18 mA cm^{-2}, and 56 mA cm^{-2} at the potential of 720 mV (Fig. 6a). In the case of Ni and Co complexes, graphitized carbon cloth enhances the catalytic performance due to the carbon cloth's conducting and porous nature. The porosity determines the ease of accessibility (pore dimensions) of the active sites and affects the mass transport.[23] Current density (j) is a measure of rate of the reaction, which in turn is proportional to the number of active sites on the electrode surface.[24] The porousness of the hybrid electrocatalyst on carbon cloth has a pore diameter of 37 ± 5 μm, while bare carbon cloth has a pore diameter of 42 ± 5 μm. The results implied that the porous electrode shows much higher (j) compared to planar systems of similar dimensions.[25] The enhanced electrocatalytic activity exhibited by the hybrid catalyst complex can be ascribed to the synergistic effect of the M(II)BTT complex and graphitized carbon cloth. The weaved textile-like property with graphite exposes a large fraction of active surface area, in turn enlarging the contact area with the electrolyte accelerating the diffusion. These factors favor excellent electrocatalytic activity for the HER.

Tafel slopes were obtained from linear sweep voltammetry measurements by plotting potential as a function of log j using the relation $\eta = a + b \log j$.[26] The Tafel slope values reveal the kinetics of the HER reaction. The Tafel slope value of 73.74 mV dec^{-1} of Pd(II)BTT is comparable to the Tafel slope value of Pt/C (47.34 mV dec^{-1}) (Fig. 6c). The slope values reveal that the HER process involves the Volmer–Tafel mechanism,[27,28] where hydrogen on the electrode surface recombines with a hydronium ion to produce H$_2$. The Tafel mechanism of Pd(II)BTT/GrCC, Co(II)BTT/GrCC, and Ni(II)BTT/GrCC exhibited high Tafel slope values of 144 mV dec^{-1}, 410 mV dec^{-1}, and 165 mV dec^{-1}, respectively (Fig. 6d) indicating sluggish reaction kinetics and obey Volmer–Heyrovsky as the possible mechanistic pathway.[29,30] To understand the high catalytic activity of the Pd, Co, and Ni complexes, the double-layer capacitance was measured. Cyclic voltammetry was performed at different scan rates ranging from 20 to 200 mV and the plot of $\Delta j (j_a - j_c)$ against the scan rate yielded the slope value (C_{dl}). The hybrid
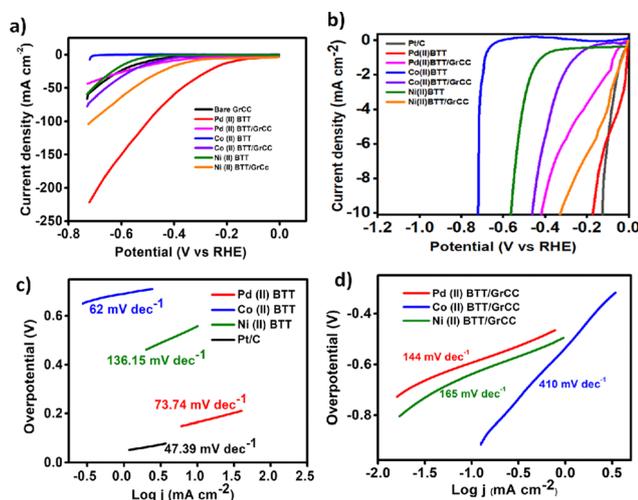
Fig. 6 (a) Linear sweep voltammetry curves of pristine M(II)BTT and M(II)BTT/GrCC complexes in the acid electrolyte at a scan rate of 50 mV s^{-1}. (b) Comparison plot of the linear sweep voltammetry curve of 10% Pt/C and M(II)BTT, M(II)BTT/GrCC at 10 mA cm^{-2} in acidic conditions. (c) Tafel slopes of the linear polarization curves of pristine M(II) complexes and Pt/C. (d) Tafel slopes of the linear polarization curves of the M(II)BTT/GrCC complexes.

catalyst showed a C_{dl} value of 12.06 mF cm^{-2}, 26.19 mF cm^{-2}, and 8.94 mF cm^{-2} for the Pd, Co, and Ni complexes on GrCC, respectively (Fig. 7b). The electrochemical active surface area (ESCA) is a good descriptor of the electrochemical activity toward the hydrogen evolution reaction. The ECSA was determined from eqn (2), and the double-layer capacitance current is directly proportional to the electrochemical active surface area (ECSA).[31] The linearity obtained from the plot of geometrical current density and scan rate revealed a diffusion-controlled electrocatalytic process. The facile electron flow in the process is due to diffusion.

$$C_{dl} = \frac{\Delta j}{v} \quad (1)$$

$$ECSA = \frac{C_{dl}}{C_s} \quad (2)$$

where Δj is current density (mA cm^{-2}), and V is potential. C_s is the specific capacitance (C_s = 0.04 mF cm^{-2}).[32] Pd(II)BTT/GrCC, Co(II)BTT/GrCC and Ni(II)BTT/GrCC hybrid complexes involve an ECSA value of 3.015 m^2 g^{-1}, 2.235 m^2 g^{-1} and 6.547 m^2 g^{-1}, respectively. The high surface area of the electrocatalysts is due to the carbon cloth's porous and woven textile framework. In order to evaluate the electrode kinetics of the HER process, electrochemical impedance spectroscopy (EIS) was performed within the frequency range of 100 kHz to 10 mHz. The Nyquist plots for all the complexes were obtained with a signal amplitude perturbation of 10 mV. As can be seen from Fig. 7d, both hybrid and pristine complexes exhibited a single capacitive loop indicating the charge transfer process as the rate-determining step (RDS). The diameter of the semicircle directly correlates with the charge transfer resistance (R_{ct}). From Fig. 7d, Pd(II)BTT showed the least charge transfer resistance of 90 ohms suggesting superior kinetics over the rest of the complexes. However, the Pd(II)BTT/GrCC, Co(II)BTT/GrCC and Ni(II)BTT/GrCC complexes exhibited relatively high charge transfer resistance of 190, 480 and 830 ohms, respectively. The hybrid catalyst of Co(II) and Ni(I) showed favourable kinetics towards hydrogen evolution compared to the pristine complexes. The details of the proposed mechanism for the hydrogen evolution reaction have been described in Section S8 (ESI†). The general hydrogen evolution reaction follows the proton coupled electron transfer mechanism (PCET) shown in Fig. 8a.[20]

Carbon supports have been extensively used to enhance the durability of electrocatalysts.[33] The metal complexes were subjected to linear sweep voltammetry in N$_2$ saturated 0.5 M H$_2$SO$_4$ before and after 6 h of chronoamperometry (Fig. 7c). The durability of the electrodes during the HER process was investigated using chronoamperometry. A constant potential was applied to the electrode for 6 h. As can be seen from Fig. 9(a–c), the hybrid catalysts showed good durability with the current density decreasing after 4 h. From Fig. 9a, the Pd complex (η = 0.410 V) showed excellent stability for 6 h with 85% current density retention activity compared to the Co and Ni complex, which showed a drop in the current density value after 4 h (Fig. 9b and c). In contrast, the Co(II) and Ni(II) hybrid catalyst activity gradually diminished after 4 h (Fig. 8b and c). The durability has been one of the prominent limitations with respect to molecular complexes. The durability of the complex can be improved further with better carbon support materials.[34]
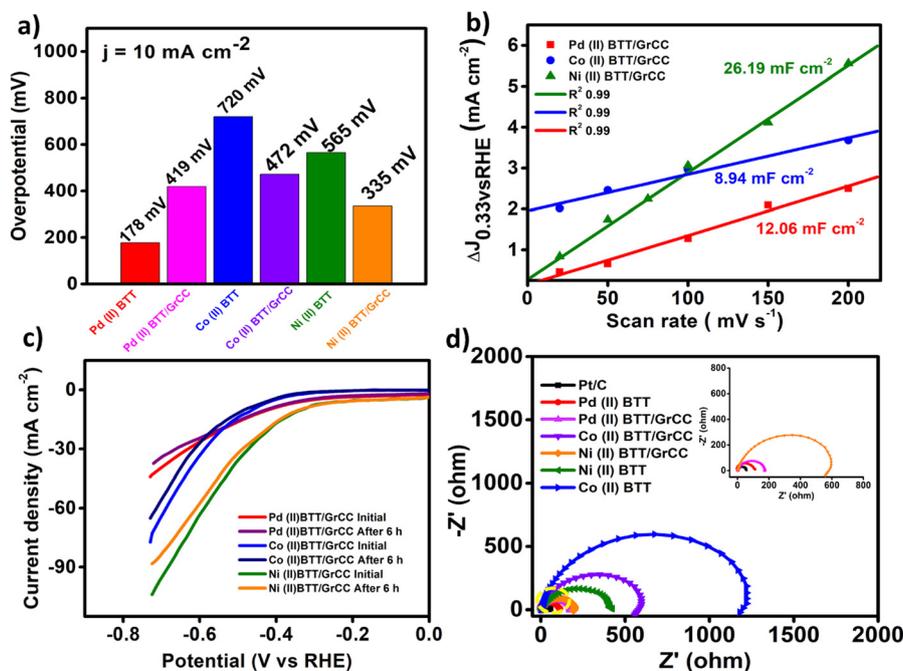

Fig. 7 (a) Overpotentials to produce a current density of 10 mA cm^{-2} under acidic conditions. (b) Evaluation of the double layer capacitance (C_{dl}) of the M(II)BTT complexes in 0.5 M H$_2$SO$_4$. (c) Stability study through linear polarization curves for 6 h in acid electrolyte. (d) Nyquist plot of M(II)BTT and M(II)BTT/GrCC complexes obtained at the corresponding onset potentials.
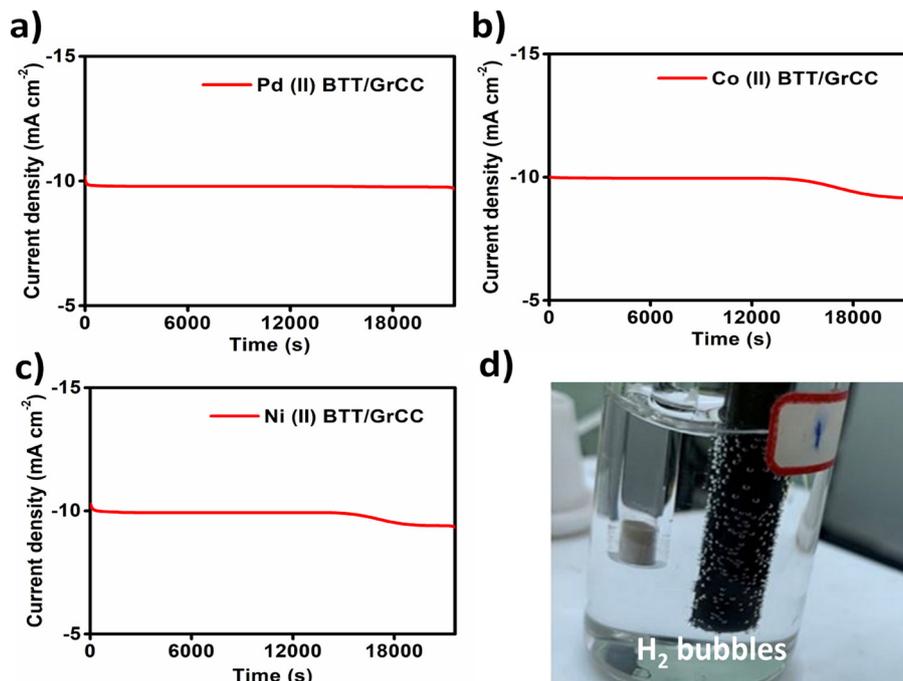
Fig. 8 (a) Durability test performed for M(II)BTT by the chronoamperometry technique at a constant potential: (a) Pd(II)BTT/GrCC −0.410 V, (b) Co(II)BTT/GrCC −0.472 V and (c) Ni(II)BTT −0.335 V. (d) Digital photograph depicting the hydrogen evolution reaction from the experimental set up in 0.5 M H_2SO_4.

2.2 Oxygen evolution reaction

The three complexes were also evaluated for their oxygen evolution reaction (OER) activity using a standard three-electrode cell with a rotating disk electrode (RDE) as the working electrode, graphite rod as an auxiliary electrode, and mercury/mercury oxide as the reference electrode. The OER reaction was carried out in 0.1 M KOH solution with a rotation rate of 1600 rpm in oxygen saturated environments. The LSV curves obtained were
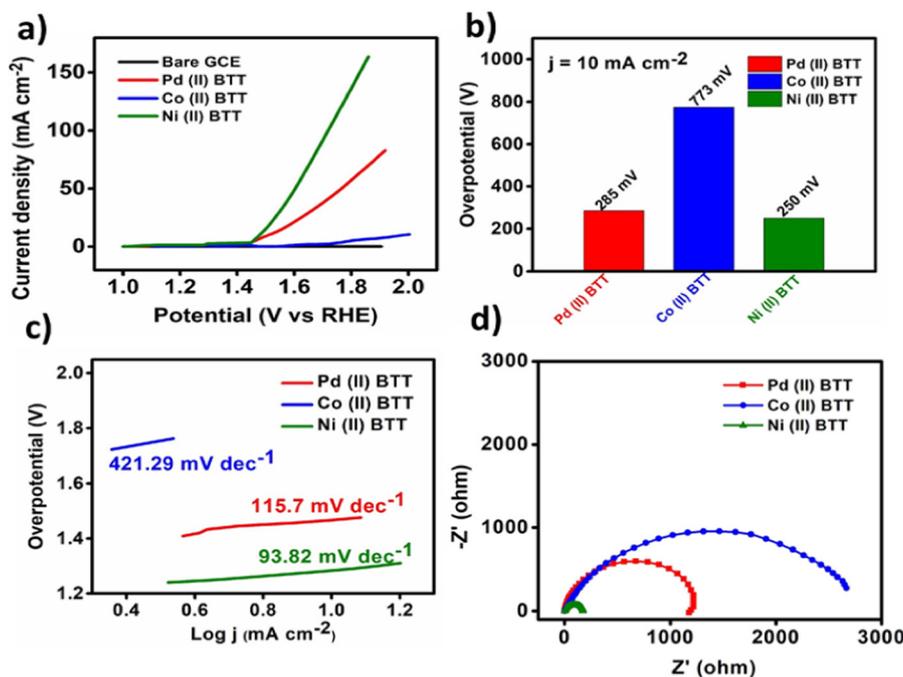

Fig. 9 (a) Linear sweep voltammetry curves of Pd(II)BTT, Co(II)BTT, and Ni(II)BTT complexes in 0.1 M KOH. (b) Overpotentials at a current density of 10 mA cm^{-2}. (c) Corresponding Tafel slopes of the linear polarization curves of the M(II)BTT complexes (Pd, Co, and Ni(II)) in 0.1 M KOH. (d) Nyquist plots depicting the charge transfer resistance of the M(II)BTT complexes (Pd, Co, and Ni(II)) BTT in acidic conditions.
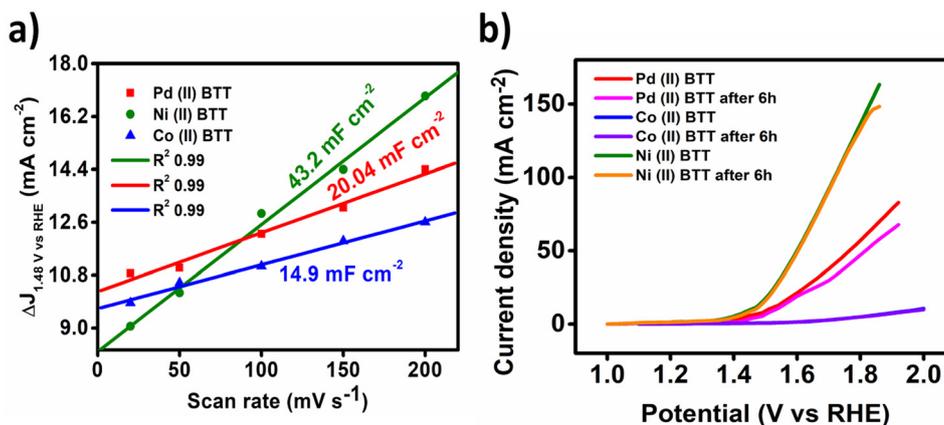
Fig. 10 (a) Determination of the double-layer capacitance value of the M(II)BTT complexes. (b) Stability study of the M(II)BTT complexes by linear polarization curves for 6 h in 0.1 M KOH.

all iR corrected with a scan rate of 50 mV s^{-1} (Fig. 10a). Fig. 10a displays the linear sweep voltammetry polarization curves. The Ni(II)BTT complex exhibited remarkably high OER performance with an overpotential of 250 mV to achieve a current density of 10 mA cm^{-2} at 1.48 V (Fig. 10a). The Co(II)BTT and Pd(II)BTT complexes exhibited an overpotential of 773 and 285 mV, respectively, to drive a current density of 10 mA cm^{-2} (Fig. 10b). The Co(II)BTT and Pd(II)BTT complexes exhibited a maximum current density of 17.12 mA cm^{-2} and 63 mA cm^{-2} at 1.98 V and 1.92 V, respectively. The Ni(II)BTT complex exhibited a maximum current density of 163 mA cm^{-2} at 1.92 V (Fig. 10a). The observed catalytic activity is due to the charge transfer from ligand to metal atoms (LMCT). From Fig. 8b, Ni(II) contains oxygen bound to a high valent metal center leading to (Ni(II)–O).

(Ni(II)–O) is a key intermediate in the oxygen evolution reaction process, which in turn reacts with H$_2$O through a water nucleophilic attack mechanism to give O–O bond formation, and the intermediate formation is the rate determining step. The reaction is aided by a hydroxide ion coupled electron transfer reaction resulting in an oxygen evolution reaction (Fig. 8b).

The Tafel slopes for all the three complexes are shown in Fig. 9c, where Ni(II)BTT showed a slope value of 93.82 mV dec^{-1}, Co(II)BTT showed 421.21 mV dec^{-1}, and the Pd(II)BTT complex showed 182.6 mV dec^{-1} (Fig. 9c). The Tafel slope values are the lowest compared to many nanocomposites[1] and other transition metal nanosheets.[35] The metal complex on the modified glassy carbon surface undergoes oxidation from Ni(0) to Ni(II), leading to reduction of the hydroxide ion to
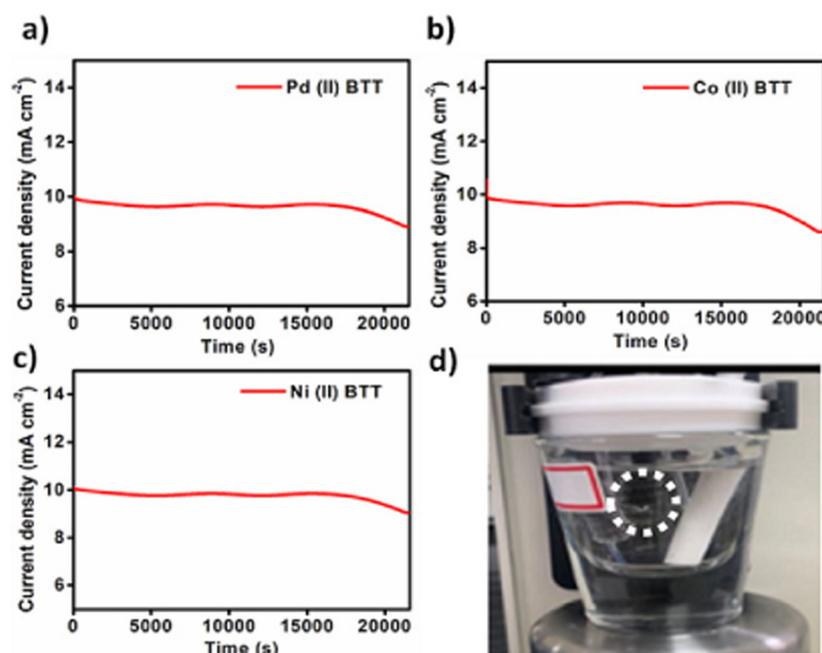

Fig. 11 Durability test performed for the M(II)BTT complexes by the chronoamperometric technique at constant potential: (a) Pd(II)BTT (1.48 V vs. RHE), (b) Co(II)BTT (2.0 V vs. RHE) and (c) Ni(II)BTT (1.52 V vs. RHE). (d) Oxygen evolution reaction image from the experimental set up in 0.1 M KOH.
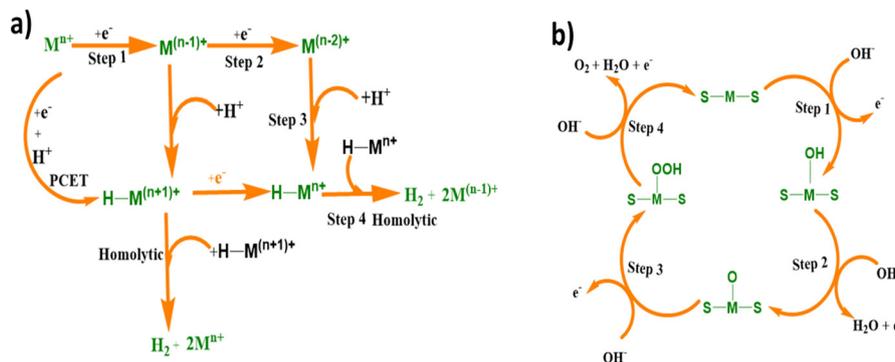
Fig. 12 (a) Mechanistic pathway of the hydrogen evolution reaction of the M(II)BTT complexes (Pd, Co and Ni). (b) Mechanism of the oxygen evolution reaction of the M(II)BTT complexes (Pd, Co and Ni).

an oxygen molecule. Hence, the Ni(II) complex showed better OER catalytic activity compared to Co(II) and Pd(II). However, in the case of the HER, the Pd(II) complex exhibited enhanced hydrogen evolution reaction activity due to the affinity of palladium towards hydrogen. The Ni and Pd complexes exhibit promising activity in terms of overpotential towards both the hydrogen and oxygen evolution reaction.

The kinetics of the oxygen evolution reaction were evaluated by impedance analysis under alkaline conditions. All three complexes' onset potential were used to obtain impedance plots. The lower the semicircle diameter, the better the electro-catalytic efficiency of the catalyst. The Ni(II) complex showed good catalytic activity with a charge transfer resistance value of 246 ohms (Fig. 9d). Pd(II) and Co(II) exhibited a charge transfer resistance of 1600 ohms and 2700 ohms, respectively, as shown in Fig. 9d. The Ni(II)BTT complex showed the least charge transfer resistance compared to the Co and Pd complexes. The catalysts showed a C_{dl} value of 20.04 mF cm^{-2}, 14.9 mF cm^{-2}, and 43.2 mF cm^{-2} for the Pd, Co, and Ni complexes, respectively (Fig. 11a), thus reinforcing the Ni complex as an excellent electrocatalyst towards the oxygen evolution reaction.

The durability of the complexes was tested using chronoam-perometric *i–t* curves (Fig. 12). From Fig. 12a–c, in the case of the Ni(II)BTT complex, it can be seen that the current density gradually decreases at 1.48 V (*vs.* RHE) after 4 h demonstrating good durability for all the three complexes. Linear sweep voltammetry was performed before and after 6 h of chronoam-perometry, and the catalysts showed 85% of current density retention capability (Fig. 11b).

3 Conclusions

In conclusion, M(II)BTT/GrCC hybrid electrocatalysts were synthesized using 2-thioureidobenzheteroazole metal complexes and graphitized carbon cloth. The hybrid catalysts were utilized for the HER and the pristine metal complexes were used for the OER. The Pd(II)BTT complex showed an outstanding overpoten-tial value of 178 mV to achieve a current density of 10 mA cm^{-2} in 0.5 M H$_2$SO$_4$. In contrast, the Ni(II)BTT/GrCC hybrid catalyst showed an overpotential value of 335 mV to drive a current

density of 10 mA cm^{-2}. The enhanced catalytic activity is due to the conducting and porous nature of the graphitized carbon cloth. Furthermore, the pristine Ni(II) complex exhibited an overpotential value of 250 mV to achieve 10 mA cm^{-2} for OER activity. The Ni(II) metal has strong affinity for O$_2$ molecules, leading to better oxygen evolution activity the other two metal complexes. The Ni(II)BTT complex is preferred over the other two metal complexes due to its low cost and abundance on the earth's crust. The Ni(II)BTT complex exhibited good durability with 85% current density retention capability. This work paves a new avenue to design efficient electrocatalysts in combination with more effective carbon supports for clean energy storage and conversion.

Author contributions

Ram Murthy – original manuscript writing, data curation, analysis, data interpretation revision. C. N. Sundaresan – con-ceptualization, ideation, review and editing, supervision.

Conflicts of interest

The authors declare there is no conflict of interest to report.

Acknowledgements

References

1 H. He, Y. Zhang, W. Zhang, Y. Li, X. Zhu, P. Wang and D. Hu, *ACS Appl. Mater. Interfaces*, 2022, **14**, 834–849.

2 A. P. Murthy, J. Madhavan and K. Murugan, *J. Power Sources*, 2018, **398**, 9–26.

3 L. Jia, P. Wagner and J. Chen, *Inorganics*, 2022, **10**, 53.

4 M. Shao, *J. Power Sources*, 2011, **196**, 2433–2444.

5 H. Lin, M. S. Hossain, S.-Z. Zhan, H.-Y. Liu and L.-P. Si, *Appl. Organomet. Chem.*, 2020, **34**, e5583.

6 S. Shen, Z. Wang, Z. Lin, K. Song, Q. Zhang, F. Meng, L. Gu and W. Zhong, *Crystalline-Amorphous Interfaces Coupling of CoSe2/CoP with Optimized d-Band Center and Boosted Electrocatalytic Hydrogen Evolution*, 2022.

7 M. Yu, E. Budiyanto and H. Tüysüz, *Angew. Chem., Int. Ed.*, 2022, **61**, e202103824.

8 M. Rajakumar, M. Manickam, N. N. Gandhi and K. Muthukumar, *Int. J. Hydrogen Energy*, 2020, **45**, 3905–3915.

9 V. Vij, S. Sultan, A. M. Harzandi, A. Meena, J. N. Tiwari, W.-G. Lee, T. Yoon and K. S. Kim, *ACS Catal.*, 2017, **7**, 7196–7225.

10 H. Yapati, S. R. Devineni, S. Chirumamilla and S. Kalluru, *J. Chem. Sci.*, 2016, **128**, 43–51.

11 B. Huang, L. Chen, Y. Wang, L. Ouyang and J. Ye, *Chem. – Eur. J.*, 2017, **23**, 7710–7718.

12 M. Chhetri, U. Gupta, L. Yadgarov, R. Rosentsveig, R. Tenne and C. Rao, *ChemElectroChem*, 2016, **3**, 1937–1943.

13 J. Zhang and L. Dai, *Angew. Chem., Int. Ed.*, 2016, **55**, 13296–13300.

14 J.-X. Wu, C.-T. He, G.-R. Li and J.-P. Zhang, *J. Mater. Chem. A*, 2018, **6**, 19176–19181.

15 D. K. Singh, R. N. Jenjeti, S. Sampath and M. Eswaramoorthy, *J. Mater. Chem. A*, 2017, **5**, 6025–6031.

16 W. Zhou, J. Jia, J. Lu, L. Yang, D. Hou, G. Li and S. Chen, *Nano Energy*, 2016, **28**, 29–43.

17 H. Shi, G. Wen, Y. Nie, G. Zhang and H. Duan, *Nanoscale*, 2020, **12**, 5261–5285.

18 S. Niu, W. Guo, T.-W. Lin, W. Yu, Y. Wu, X. Ji and L. Shao, *RSC Adv.*, 2017, **7**, 25885–25890.

19 A. K. El-Sawaf, F. El-Essawy, A. A. Nassar and E.-S. A. El-Samanody, *J. Mol. Struct.*, 2018, **1157**, 381–394.

20 M. Drosou, F. Kamatsos and C. A. Mitsopoulou, *Inorg. Chem. Front.*, 2020, **7**, 37–71.

21 Z. Zong, K. Xu, D. Li, Z. Tang, W. He, Z. Liu, X. Wang and Y. Tian, *Peptide templated Au@Pd core-shell structures as efficient bi-functional electrocatalysts for both oxygen reduction and hydrogen evolution reactions*, 2018.

22 T. Wang, D. Gao, J. Zhuo, Z. Zhu, P. Papakonstantinou, Y. Li and M. Li, *Chem. – Eur. J.*, 2013, **19**, 11939–11948.

23 P. Adler, *Porous media: geometry and transports*, Elsevier, 2013.

24 J. Haverkort, *Electrochim. Acta*, 2019, **295**, 846–860.

25 A. J. Bard, L. R. Faulkner and H. S. White, *Electrochemical methods: fundamentals and applications*, John Wiley & Sons, 2022.

26 Q. Yin, Z. Xu, T. Lian, D. G. Musaev, C. L. Hill and Y. V. Geletii, *Catalysts*, 2021, **11**, 87.

27 J. Chen, H. Wang, Y. Gong and Y. Wang, *J. Mater. Chem. A*, 2019, **7**, 11038–11043.

28 Z. Lin, B. Xiao, M. Huang, L. Yan, Z. Wang, Y. Huang, S. Shen, Q. Zhang, L. Gu and W. Zhong, *Adv. Energy Mater.*, 2022, 2200855.

29 L. Yang, Y. Lv and D. Cao, *J. Mater. Chem. A*, 2018, **6**, 3926–3932.

30 S. Shen, Z. Hu, H. Zhang, K. Song, Z. Wang, Z. Lin, Q. Zhang, L. Gu and W. Zhong, *Angew. Chem., Int. Ed.*, 2022, **61**, e202206460, DOI: 10.1002/ange.202206460.

31 Y.-H. Choi, *Nanomaterials*, 2022, **12**, 939.

32 V.-T. Nguyen, H. Ha, N.-A. Nguyen, H. An, H. Y. Kim and H.-S. Choi, *ACS Appl. Mater. Interfaces*, 2020, **12**, 15500–15506.

33 Z. Lin, B. Xiao, M. Huang, L. Yan, Z. Wang, Y. Huang, S. Shen, Q. Zhang, L. Gu and W. Zhong, *Adv. Energy Mater.*, 2013, **12**, 2200855.

34 S. Manzoor, S. V. Trukhanov, M. N. Ansari, M. Abdullah, A. Alruwaili, A. V. Trukhanov, M. U. Khandaker, A. M. Idris, K. S. El-Nasser and T. A. Taha, *Flowery ln2MnSe4 Novel Electrocatalyst Developed via Anion Exchange Strategy for Efficient Water Splitting*, 2022.

35 R. Elakkiya and G. Maduraiveeran, *Langmuir*, 2020, **36**, 4728–4736.